International Journal of Fatigue 170 (2023) 107509

Contents lists available at ScienceDirect

International Journal of Fatigue

journal homepage: www.elsevier.com/locate/ijfatigue

Bonded and additively manufactured crack retarders: A comparative study of damage tolerance properties

Václav Jetela [a,*], Josef Klement [a], Jakub Holzer [b], Ján Kondás [c,d]

[a] Institute of Aerospace Engineering, Brno University of Technology, Technická 2896/2, 61600 Brno, Czech Republic
[b] Institute of Physics of Materials of the Czech Academy of Sciences, Žižkova 513/22, 61600 Brno, Czech Republic
[c] Impact Innovations GmbH, Bürgermeister-Steinberger-Ring 1, 84431 Rattenkirchen, Germany
[d] Department of Mechanical Engineering, Politecnico di Milano, Via Privata Giuseppe La Masa 1, 20156 Milano, Italy

ARTICLE INFO

Dataset link: http://dx.doi.org/10.17632/xvmwtj8hr9.1

Keywords:
Bonded crack retarder
Cold spray
Ultrasonic consolidation
Fatigue crack growth
Integral airframe structure

ABSTRACT

Fatigue crack grows faster in the integral structure than in the riveted structure. This study compares the bonded, cold-sprayed and ultrasonically consolidated crack retarders to increase the fatigue life of integral airframe structure. The 2024-T351 aluminum M(T) specimen reinforced with crack retarders made of AISI 301 and 316L steels, Ti–6Al–4V titanium alloy and unidirectional CFRP laminate are evaluated in terms of fatigue life, delamination resistance and weight efficiency. Specimens were subjected to constant amplitude loading up to the final failure. A substantial decrease in fatigue crack growth rate was achieved using the ultrasonically consolidated AISI 301 crack retarder.

1. Introduction

The integral airframe structure saves weight and contains fewer stress concentrations but does not contain physical barriers against fatigue crack growth. The physical barrier is classified as a place in a structure where one part of a structure is covered by another part. If the physical barriers are non-existent, the fatigue crack can grow from one integral element to another without delay. It results in earlier fatigue failure of integral structure [1].

One of the techniques to slow down crack propagation is the application of so-called "crack retarders". These selective reinforcements are usually made of materials with different mechanical properties than the base structure material. Their role is to reduce the crack opening through the bridging effect [2]. The crack retarder also acts as a stiffener and transfers the load from the substrate before the crack reaches the stiffener's position.

However, the crack retarder may start delaminating in front of the progressing crack tip, where the maximum tensile stresses are, and/or at the free ends, where the maximum shear stresses are. The retarder can still carry the load but is less effective due to the lack of shear transfer capability [3]. Crack retarders are located on one side of the airframe structure; the structure's central axis is shifted. As the unsymmetrical structure is tension loaded, the bending moments emerge and cause out-of-plane deformation [4], which results in a stress increase at the crack tip. Suppose coefficients of thermal expansion of substrate and crack retarder deviate. In that case, the change in ambient temperature (manufacturing process, service conditions) promotes residual thermal stresses [5] that may affect stress at the crack tip. Another issue to be addressed is galvanic corrosion when combining dissimilar materials and crack retarder fatigue sensitivity.

Previous studies demonstrated a promising increase in fatigue life when using crack retarders made of ARALL fiber metal laminate [6], Al_2O_3/Al metal matrix composite [7], CFRP laminates [3,8], Ti–6Al–4V alloy [9], GLARE fiber metal laminate [10,11], cold-sprayed 7075 alloy [12] and ultrasonically consolidated Al_2O_3/Al metal matrix composite [13]. Furthermore, crack retarders were extensively evaluated in terms of residual thermal stresses after curing [14–16]; their durability (impact damage, thermal cycling) [17,18] and optimal design parameters [19].

A solid-state joint can be achieved between dissimilar metals using cold spray and ultrasonic consolidation. Cold spray is the technology that allows depositing thick metallic and non-metallic coatings. In this process, compressed and heated gas is used to carry particles through the de Laval nozzle. As the mixture expands, the velocity of particles increases. The particles then impact the substrate and create a metallurgical bond with the substrate and/or other particles [20]. Ultrasonic

Abbreviations: BCR, Bonded Crack Retarder; BCRs, Bonded Crack Retarders; CF, Carbon Fiber; CSCR, Cold-Sprayed Crack Retarder; CSCRs, Cold-Sprayed Crack Retarders; CTE, Coefficient of Thermal Expansion; UCCR, Ultrasonically Consolidated Crack Retarder; UD, Unidirectional

* Corresponding author.
E-mail address: Vaclav.Jetela@vutbr.cz (V. Jetela).

https://doi.org/10.1016/j.ijfatigue.2023.107509
Received 20 June 2022; Received in revised form 17 December 2022; Accepted 6 January 2023
Available online 9 January 2023

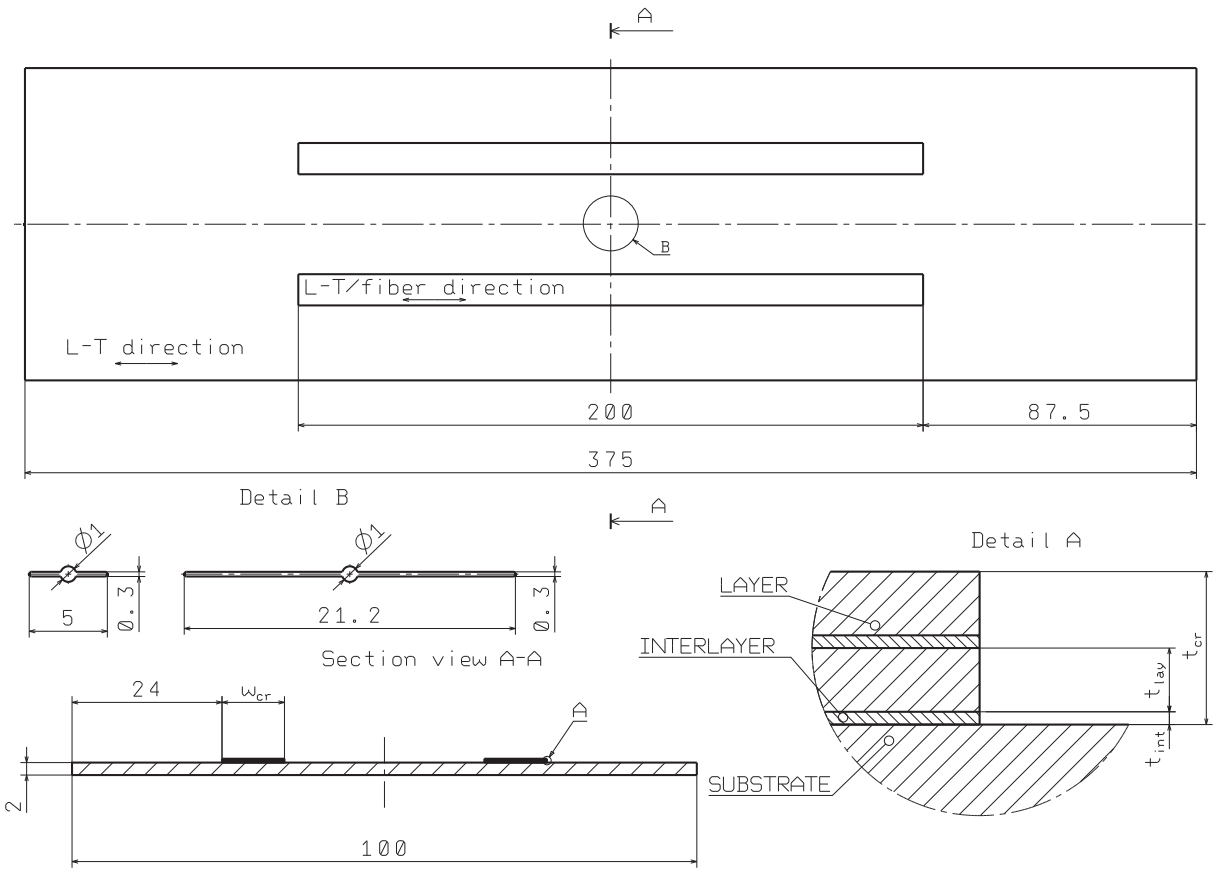

Fig. 1. Specimen shape. Dimensions in millimeters, not in scale. Specimens with CSCR and BCR: 5 mm long notch. Specimens with UCCR: 21.2 mm long notch.

Table 1
2024-T351 chemical composition [25].

Alloy	Al	Cr	Cu	Fe	Mg	Mn	Si	Ti	Zn
2024 -T351	Bal.	≤0.1	3.8 4.9	≤0.5	1.2 1.8	0.3 0.9	≤0.5	≤0.15	≤0.25

consolidation is the process of continuous ultrasonic welding. It uses the mechanical vibrations and normal force of sonotrode to remove the oxide layer between two metallic foils. As the sonotrode rotates, it creates the metallurgical bond along the predefined path [21]. In as-built condition, the shear strength of ultrasonically consolidated Al–Ti joint [22,23] and cold-sprayed AISI 316L-Al joint [24] has reached or exceeded the maximum shear strength of adhesive joints. We hypothesize that crack retarders manufactured using these two additive technologies might outperform bonded crack retarders. It has been demonstrated only for material combination (Al retarder on Al substrate) that due to the excellent adhesion of cold-sprayed crack retarders, the fatigue life of the specimen can be increased [12]. However, cold-sprayed crack retarders made of a different material from the substrate have not been evaluated in terms of their performance. This study also investigates the performance of ultrasonically consolidated crack retarders since only one study focused on the Al_2O_3/Al metal matrix composite [13] has been found.

Due to the combination of the CTE close to the substrate's value and high elastic modulus, stainless steel was chosen as the material for the crack retarders. The combination of such material properties might increase the crack retarder's performance. For comparison purposes, the CF UD laminate was included in this study because it has proven outstanding crack-retarding abilities.

2. Manufacturing methods

2.1. Substrate

The M(T) specimens (Fig. 1) were high-speed milled from the sheet made of 2024-T351 aluminum alloy (Table 1), which is widely used in various aerospace applications. The bare M(T) specimens were used as a substrate for bonded and cold-sprayed crack retarders and as a reference specimen for comparison purposes. The M(T) specimen width and length were chosen according to ASTM E647 [30] while the thickness of 2 mm represented the typical integral wing skin panel. The mechanical properties of substrate are shown in Table 2. In the case of specimens with ultrasonically consolidated crack retarders, the substrate was manufactured in the reverse order (as elaborated in Section 2.4). The geometry of substrate for consolidated crack retarders and the location of consolidated crack retarders are depicted in Fig. 1. Dimensions of each crack retarder and its constituents are presented in Table A.1.

2.2. Bonded crack retarders

2.2.1. Austenitic stainless steel

Previous studies on crack retarders for aerospace applications excluded steels due to the higher specific weight that could result in high fuel consumption and CO_2 emissions. However, the stainless steels possess the CTE close to the aluminum alloy in combination with excellent tensile strength and elastic modulus. Hence, the austenitic stainless steel AISI 301 in the work-hardened state was selected for this study (see Table 2, 3 for mechanical properties and chemical composition). The capability of retarding the crack growth was examined using specimens with one bonded steel layer and two bonded steel layers.

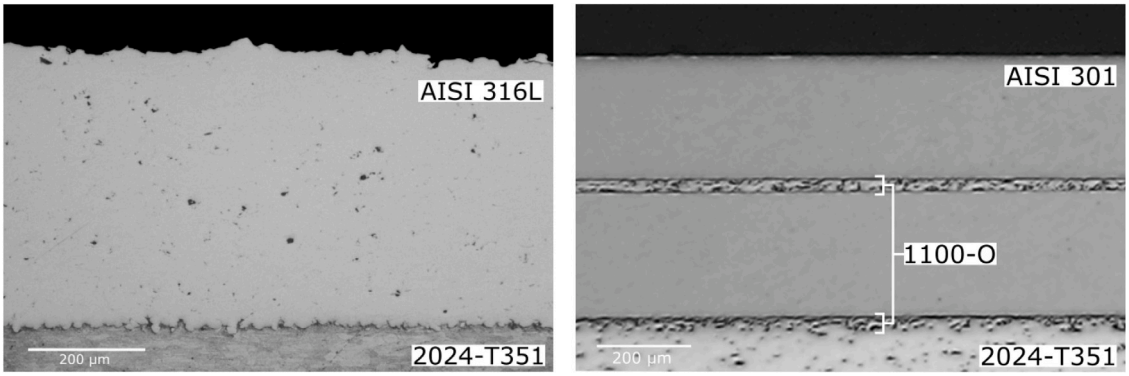

(a) 1-AISI316L-CSCR specimen: cold-sprayed AISI 316L crack retarder

(b) 2-AISI301-UCCR specimen: Ultrasonically consolidated AISI 301 crack retarder

Fig. 2. Micrograph of additively manufactured crack retarders.

Table 2
Mechanical and thermal properties of substrate, bonded crack retarder and adhesive.

Material		2024-T351[a]	AISI 301	M10R/38% /UD150/CHS	Araldite® 2011
Young's modulus	E [GPa]	72.4	185[b]	136[d] /143[e]	1.9[h]
Density	ρ [g/cm^3]	2.77	7.88[c]	1.57[f]	1.05[h]
CTE	α [10^{-6}/K]	23	17[c]	1[g]	–
Tensile strength	Rm [MPa]	470	1635[b]	2168[d] /2676[e]	–
Yield strength	$Rp_{0.2}$ [MPa]	325	1508[b]	–	–
Elongation	A [%]	20	2.1[b]	–	–

[a] [25].
[b] [26].
[c] [27].
[d] Two layers. Tested according to ASTM D3039.
[e] Five layers. Tested according to ASTM D3039.
[f] [28].
[g] Typical generic values.
[h] [29].

Table 3
AISI 301 chemical composition [27].

Alloy	Fe	C	Mn	Si	P	S	Cr	Ni
AISI 301	Bal.	≤0.15	≤2	≤1	≤0.045	≤0.03	16 18	6 8

Table 4
SANDVIK 316L (15–38 µm) powder chemical composition [31].

Alloy	Fe	C	Cr	Ni	Mo	Si	Mn	S	P
AISI 316L	Bal.	≤0.03	16.0 18.0	10.0 14.0	2.0 3.0	≤1.0	≤2.0	≤0.03	≤0.045

Crack retarder surface pretreatment. The straps used for adhesive bonding of crack retarders were cut out of the sheet made of 0.255 mm thick AISI 301 steel and degreased with acetone. Subsequently, they were immersed in the solution containing 12.5% HF, 40.8% H_2O, and 46.7% HNO_3 for 20 min at the ambient temperature. In the end, rinsing with water and blow-drying with the 45 °C air took place.

Adhesive bonding. The crack retarders were bonded to the specimen surface using the two-component Araldite® 2011 structural adhesive. The specimen with one steel layer (1-AISI301-BCR) was cured for 24 h at the ambient temperature and 30 min at 80 °C. In the case of the specimen with two steel layers (2-AISI301-BCR), first, two pretreated straps were bonded together and cured. An excessive adhesive layer on the outer surfaces was removed. Then, the resulting BCRs were degreased with acetone and immersed in the solution containing H_2O, HF and HNO_3 for 20 min at the ambient temperature. Finally, bonding onto the substrate and curing were done. The same curing process was used as in the case of the 1-AISI301-BCR. Note that two specimens with two steel layers were manufactured; specimens 2-AISI301A-BCR and 2-AISI301B-BCR.

2.2.2. Unidirectional carbon fiber

To compare the performance of steel crack retarders with previously validated crack retarder material, the specimens with BCRs made of two (1-CFUD-BCR) and five layers (2-CFUD-BCR) of M10R/38%/UD150 /CHS prepreg were prepared. The prepreg consists of the high-strength unidirectional 12 K carbon fiber fabric and the M10R epoxy resin matrix (see mechanical properties in Table 2).

Crack retarder manufacturing process. First, the prepreg roll was defrozen at the ambient temperature to avoid the condensation of air humidity. Then, the individual prepreg plies were cut out of the prepreg roll. After removing the release film from the prepreg plies, the desired number of prepreg plies was positioned in a single direction. Then the entire assembly was covered with the peel ply, bleeder cloth and vacuum bagging film. This assembly was autoclaved at 5 bar and 120 °C for 1 h. Finally, the cured sheets were cut with a hand saw to obtain 10 mm wide crack retarders.

Crack retarder surface pretreatment. Using peel ply, the crack retarder surfaces were modified to optimize the bond quality. Before bonding, they were degreased with acetone.

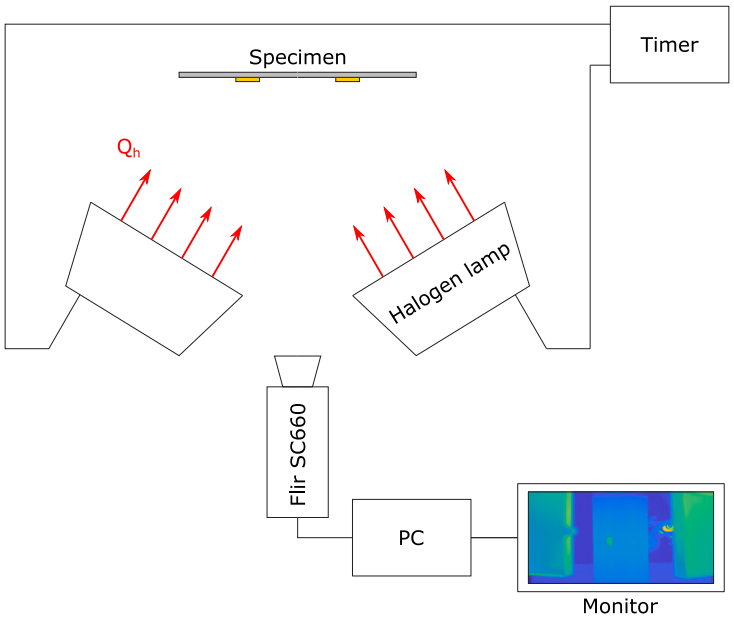

Fig. 3. Pulsed thermography apparatus.

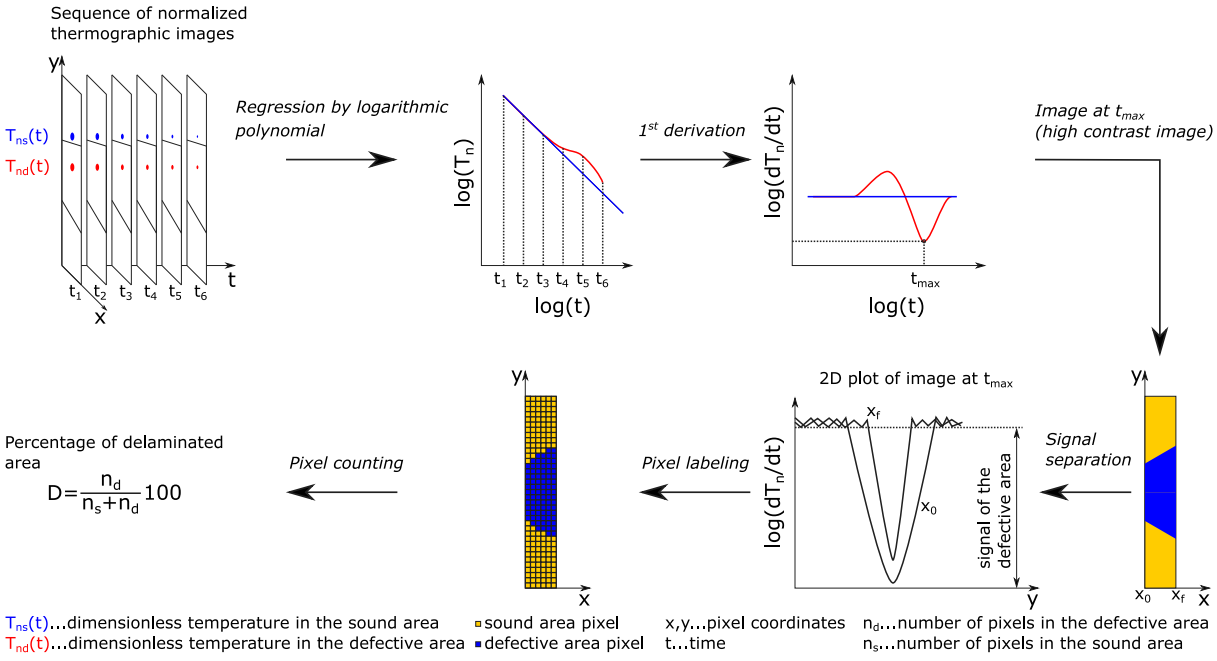

Fig. 4. Thermographic image processing.

Table 5
AP&C Ti–6Al–4V (15–45 μm) powder chemical composition [32].

Alloy	Ti	Al	V	Fe	O	C	N	H	Y
Ti–6Al–4V	Bal.	5.50 6.75	3.50 4.50	0.05 0.25	0.14 0.16	≤0.02	≤0.02	≤0.010	<0.005

Adhesive bonding. The CF UD crack retarders were bonded to the 2024-T351 substrate surface using the Araldite® 2011. The 1-CFUD-BCR specimen and 2-CFUD-BCR specimen were first cured for 24 h at the ambient temperature and then cured for 30 min at 80 °C. Admittedly, combining the carbon fiber laminate with aluminum alloy might lead to galvanic corrosion and the hot curing process introduced residual thermal stresses to the specimen.

2.3. Cold-sprayed crack retarders

To compare the bonded crack retarders with cold-sprayed ones, two specimens with alpha-beta alloy Ti–6Al–4V and two with austenitic stainless steel AISI 316L crack retarders were manufactured (see Tables 4 and 5 for powder properties). Crack retarders were deposited (Fig. 2(a)) using the Impact Spray System 5/11 and optimized process

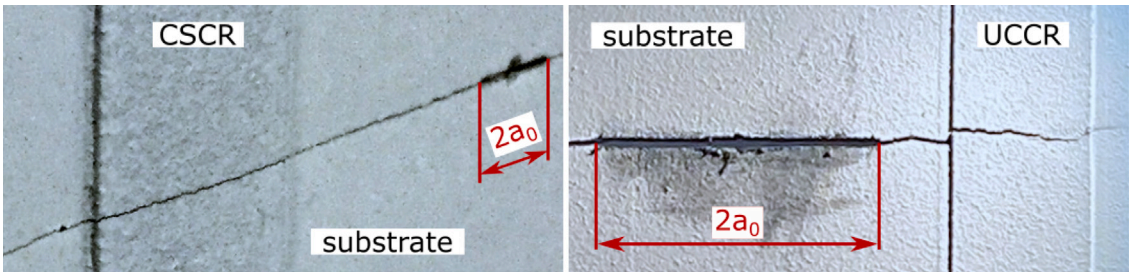

(a) Specimen 1-AISI316L-CSCR. Cold-Sprayed Crack Retarder (CSCR). (b) Specimen 1-AIS301-UCCR. Ultrasonically Consolidated Crack Retarder (UCCR).

Fig. 5. Direct propagation of fatigue crack to crack retarder.

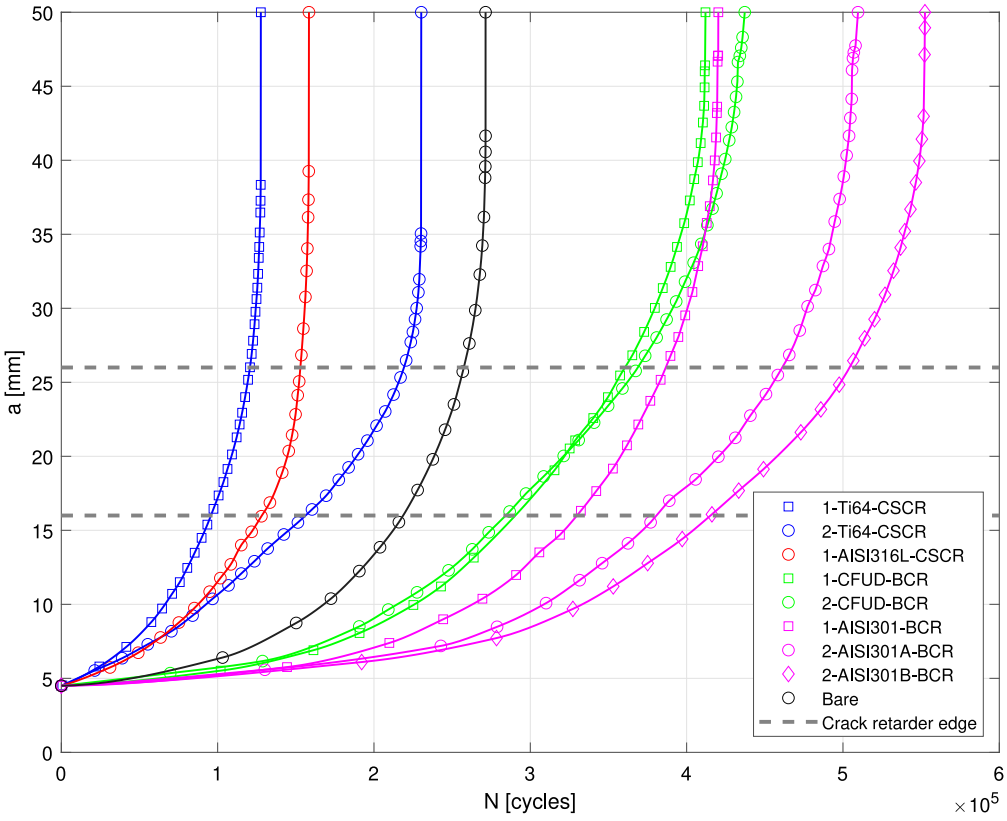

Fig. 6. Crack growth curves: bonded and cold-sprayed crack retarders; $\sigma_{max} = 60$ MPa, $R = 0.1$, $f = 15$ Hz.

parameters: stand-off distance 30 mm, step distance 1 mm, gun travel speed 0.5 m s^{-1}, gas (N_2) pressure 50 bar and temperature 1100 °C. As overspray protection, the metal mask was utilized to obtain consistent width and length of crack retarders.

Cold-sprayed deposits in as-sprayed condition often possess lower mechanical properties (Table 6) than wrought counterparts. To increase retarders' load transfer capacity, their height was increased to 0.5 mm (1-AISI316L-CSCR and 1-Ti64-CSCR specimens) and 1.0 mm (2-AISI316L-CSCR and 2-Ti64-CSCR specimens).

2.4. Consolidated crack retarders

Two 2024-T351 M(T) specimens with ultrasonically consolidated crack retarders were manufactured. The capability of retarding the crack growth was examined for the specimens with crack retarders consisting of one and two steel layers. Crack retarders were made of AISI 301 steel; the same composition, thickness and batch as in the case of BCRs.

Table 6
Mechanical and thermal properties of cold-sprayed crack retarder.

Material		Ti–6Al–4V	AISI 316L
Young's modulus	E [GPa]	69.7[a]	182[a]
Porosity	ϕ [%]	1.1/1.8[b]	0.7/1.0[b]
CTE	α [10^{-6}/K]	8.6[b]	15.9[c]
Tensile strength	Rm [MPa]	295[a]	795[a]
Yield strength	$Rp_{0.2}$ [MPa]	–	765[a]
Elongation	A [%]	0.05[a]	0.05[a]

[a]ASTM E8 Sheet-Type Subsize Specimens with 6 × 3 [mm] reduced section were used.
[b]At least five images of each cold-sprayed material were evaluated utilizing optical microscope and thresholding technique.
[c][27].

The substrate surface had to be machined before consolidation to be perfectly leveled and clean. For this reason, using the same batch of 2024-T351 bare M(T) specimens was not possible as in previous experiments. Before consolidation, the 6.35 mm thick 2024-T351 sheet was

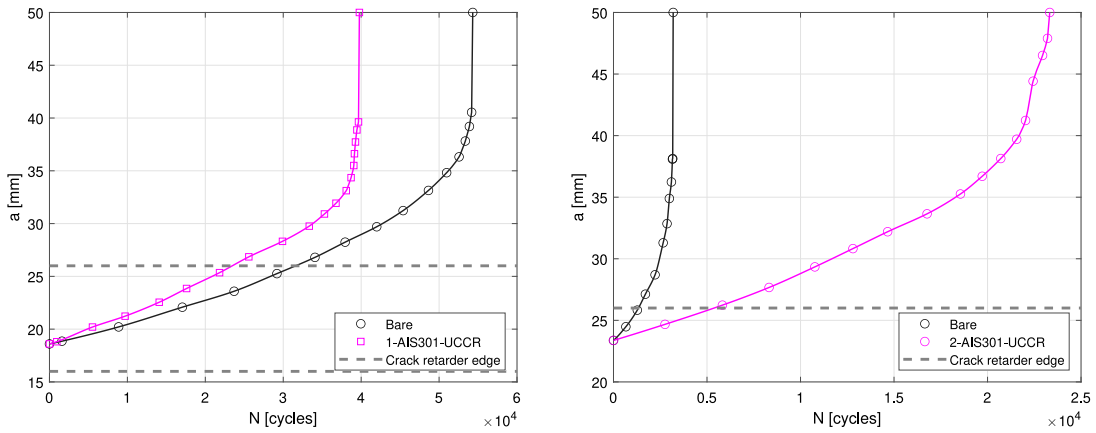

(a) Specimen 1-AISI301-UCCR; $\sigma_{max} = 60$ MPa, $R = 0.1$, $f = 15$ Hz (b) Specimen 2-AISI301-UCCR; $\sigma_{max} = 100$ MPa, $R = 0.1$, $f = 15$ Hz.

Fig. 7. Crack growth curve: ultrasonically consolidated crack retarders.

Table 7
Mechanical and thermal properties of 1100-O interlayer used in consolidated crack retarder.

Material		1100-O
Young's modulus	E [GPa]	69.0[a]
Density	ρ [g/cm^3]	2.71[a]
CTE	α [10^{-6}/K]	23.6[a]
Tensile strength	Rm [MPa]	90[a]
Yield strength	$Rp_{0.2}$ [MPa]	35[a]
Elongation	A [%]	40[a]

[a] [33].

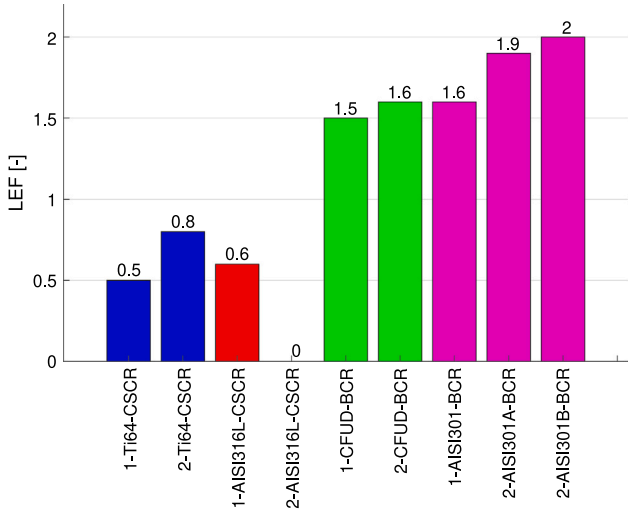

Fig. 8. Life extension factor: bonded and cold-sprayed crack retarders.

milled down to 6 mm. Crack retarders were consolidated on the milled surface. Specimens (1-AISI301-UCCR, 2-AISI301-UCCR) were then extracted from the sheet. Additionally, 2024-T351 bare M(T) specimens were extracted for comparison purposes and to avoid batch-to-batch inconsistency.

2.4.1. Austenitic stainless steel

There are two approaches to consolidate foils made of materials with a hard oxide film (e.g. stainless steels): increasing the process parameters (normal force, amplitude) and/or using the relatively soft interlayer. The former approach can cause the foil to bond with the sonotrode or lead to the sonotrode's excessive wear [34]. The latter causes the interlayer material to flow around hard oxide film resulting in the bond between two materials with hard oxide film [35]. In this study, the 0.05 mm thick 1100-O interlayer was used between AISI 301 layers (Table 7). Crack retarders were deposited (Fig. 2(b)) using the Fabrisonic SL 7200, Ultrasonic Additive Manufacturing machine with the 9 kW ultrasonic welding system. The following optimized process parameters were used: 20 kHz frequency, 40 µm amplitude, 21.2 mm/s longitudinal speed, 7500 N down force, anvil heated at 52 °C, titanium driver. The driver was placed between the sonotrode and the foil to be consolidated. It holds foil in place, transfers the horn's oscillations and prevents foil from bonding to the horn.

3. Test methods

Fatigue crack growth test. Prior testing, the initial notch ($2a_0 = 5$ mm) was machined to the specimen with bonded (CF UD, AISI 301), cold-sprayed crack retarders (Ti–6Al–4V, AISI 316L) and without crack retarder (Bare). Considerably longer notch ($2a_0 = 21.2$ mm) was machined to all specimens with ultrasonically consolidated crack retarders. The crack length was periodically measured on the specimen's unreinforced side using the traveling microscope with 32x magnification. The cyclic load was applied until the final failure of specimen. All specimens with bonded crack retarders, cold-sprayed crack retarders, without crack retarders and the specimen with ultrasonically consolidated crack retarders (1-AIS301-UCCR) were subjected to the crack propagation test with the following parameters: $\sigma_{max} = 60$ MPa, R = 0.1 and f = 15 Hz.

In the case of the 2-AIS301-UCCR specimen, the applied stress had to be increased. Even with the larger machined notch ($2a_0 = 21.2$ mm), the precracking in the 2-AIS301-UCCR specimen was unsuccessful at the $\sigma_{max} = 60$ MPa and $\sigma_{max} = 80$ MPa. The crack did not start growing after the 1.0e6 – 1.4e6 cycles. For this reason, the test was conducted at $\sigma_{max} = 100$ MPa, R = 0.1 and f = 15 Hz. At this stress level, the fatigue crack started to grow.

Delamination monitoring. Throughout the fatigue crack growth test, the thermographic inspection was carried out. After the optical excitation through 2x 400 W halogen lamps (Fig. 3), the delamination monitoring was performed by measuring the thermal response of the specimen using the Flir SC660. The thermal response was collected during heating and decay; while excitation took 5, 7 and 10 s. It appeared from the first processed thermal sequences that the highest contrast was acquired after 10 s excitation, so the analysis was performed only for this excitation time. Before testing, specimens were painted with white spray-paint ThermaSpray 500 to minimize the negative effect of reflective heat.

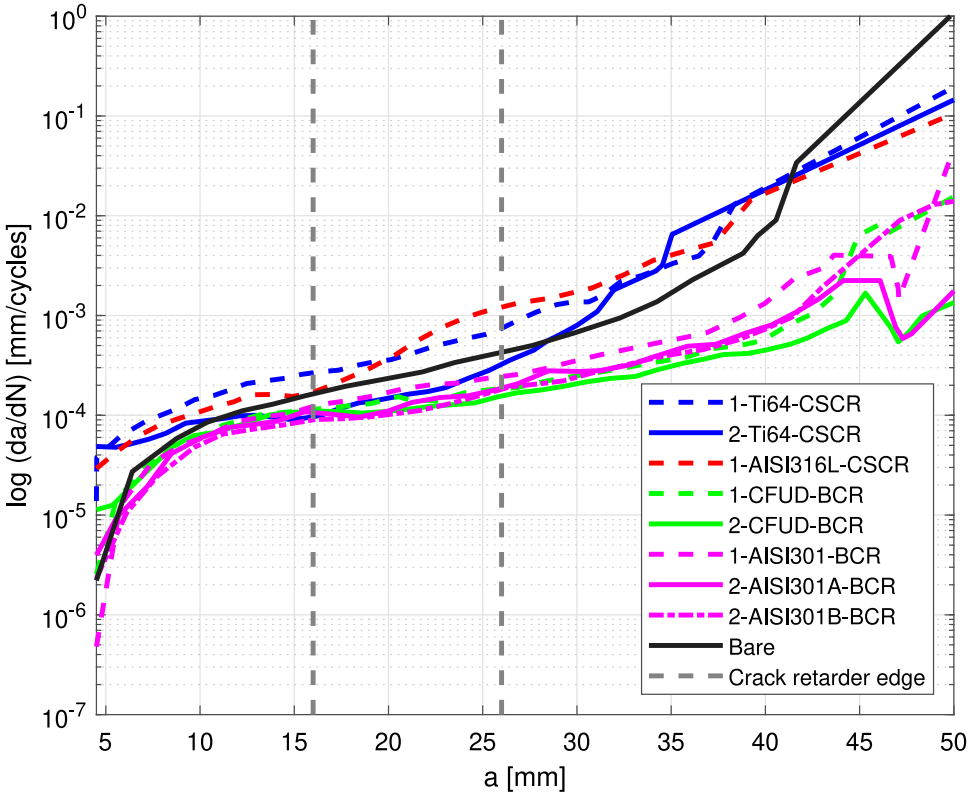

Fig. 9. Fatigue crack growth rate: bonded and cold-sprayed crack retarders.

Thermographic image processing. First, the decay sequence was extracted from the specimen's thermal response and normalized by dividing the thermal decay images by the image at the end of heating. Normalization reduced the effect of non-uniform heating and optical properties variability across the measured surface. The normalized thermal sequence was fitted with polynomials (Fig. 4) to reduce noise. By solving the first derivative of each polynomial, the contrast between the defective and the sound area was increased (i.e. Thermographic Signal Reconstruction method). From the first derivative, the time of high contrast image was found. The 2D plot was created from that image to find the defective area signal (sharp peak in the 2D plot). The pixels belonging to the defective and sound areas were sorted and counted. Finally, the delaminated area was calculated for each crack retarder.

4. Experimental results and discussion

Crack growth. During the crack propagation test, no crack initiation was observed in the BCRs. They broke[1] or disbond[2] shortly after the substrate failure. In cases of all cold-sprayed crack retarders, the crack propagated directly from the substrate to the crack retarders (Fig. 5(a)). In the case of ultrasonically consolidated crack retarders, the failure was contradictory. The fatigue crack in the specimen with one steel layer (1-AISI301-UCCR, σ_{max} = 60 MPa) directly propagated to the crack retarder (Fig. 5(b)). However, the crack in the specimen with two steel layers (2-AISI301-UCCR, σ_{max} = 100 MPa) remained in the substrate and the crack retarders broke immediately after the substrate failure. Measured crack lengths were averaged values of both crack sides and plotted against the number of cycles; thus, the crack propagation curves were obtained (Fig. 6, 7).

Regarding specimens with crack growth life longer than specimen without crack retarders (Bare), no significant delay can be observed in the crack retarder area (16–26) mm. The positive crack retarding effect manifests along the entire crack path. Similarly, any significant change in the crack growth rate cannot be observed in specimens possessing shorter fatigue life.

Fatigue life. The fatigue life improvement can be expressed by the life extension factor:

$$LEF = \frac{N_i - N_{bare}}{N_{bare}} \quad (1)$$

where N_i is the number of cycles to failure of specimen with crack retarders and N_{bare} is the number of cycles to failure of specimen without crack retarders. All bonded crack retarders resulted in a significant fatigue life extension. The greatest increase (1.9–2.0) was observed in the case of the specimen with two steel layers (Fig. 8). One can observe a relatively small difference between the fatigue crack growth curves of the specimen with two (1-CFUD-BCR) and five (2-CFUD-BCR) CF UD layers. It was probably caused by the evolution of residual thermal stresses during the curing process, which raised the mean stress and sped up the crack propagation in the specimen with thicker CF UD crack retarders. Regarding this observation, using more than two CF UD layers appears redundant. All cold-sprayed crack retarders dramatically decreased fatigue life. The most significant decrease, 50%, was observed in the fatigue life of the specimen with the Ti–6Al–4V crack retarders. The specimen with the thicker 316L crack retarder failed within the crack initiation period due to the rapidly growing crack at one of the ends of the crack retarder.

There are several explanations for the poor fatigue properties (i.e. decreased fatigue life and increased crack growth rate) of specimens with CSCRs. The substrate temperature increased due to its plastic deformation during cold spraying and heat transfer from the impinging jet. A combination of cooldown from such temperature and the crack retarder's CTE dissimilar from the substrate probably led to

[1] 1-AISI301-BCR, 1-CFUD-BCR
[2] 2-AISI301A-BCR, 2-AISI301B-BCR, 2-CFUD-BCR

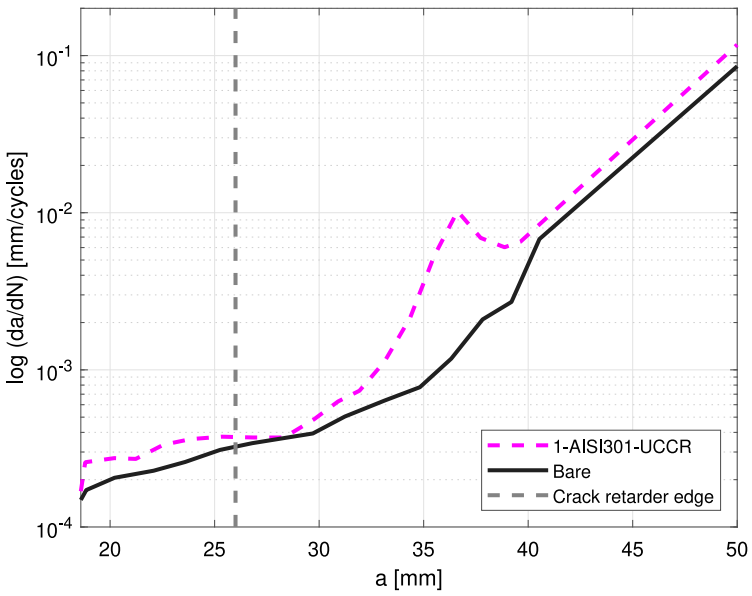

(a) 1-AISI301-UCCR specimen.

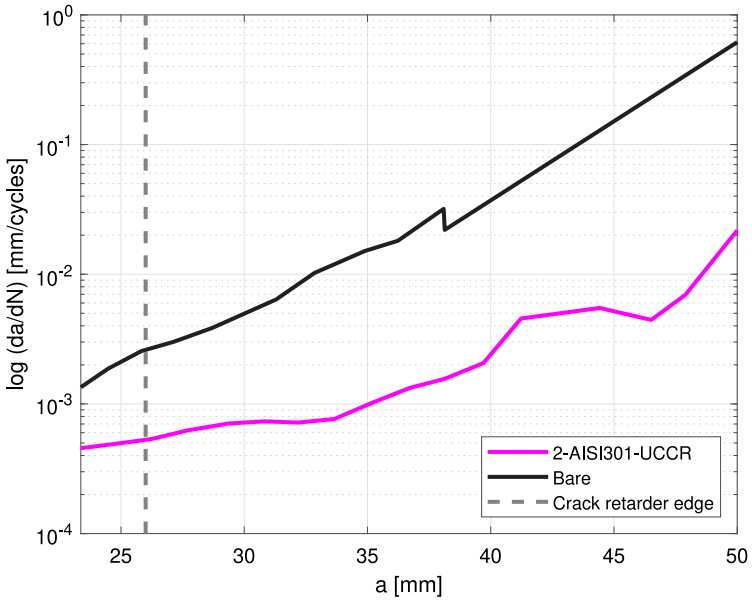

(b) 2-AISI301-UCCR specimen.

Fig. 10. Fatigue crack growth rate: ultrasonically consolidated crack retarders.

the evolution of tensile residual stresses in the substrate. Compared with Liljedahl et al.'s study [5], similar out-of-plane deformation was observed in all specimens with CSCRs. When comparing the out-of-plane deformation in all specimens with CSCRs, the greatest deflection (20.4 mm) was measured in the center of the 2-Ti64-CSCR specimen. The temperature increase in the substrate certainly altered its mechanical properties. A noticeable drop in the substrate hardness was measured in all specimens with CSCRs. For example, a 22% decrease was recorded in the substrate of 1-AISI316L-CSCR specimen.

Specimen with one ultrasonically consolidated steel layer (1-AISI301-UCCR) failed earlier; its fatigue life was 30% lower than the specimen without crack retarder (Bare). However, the specimen with two steel layers (2-AISI301-UCCR) experienced the most significant fatigue life increase by a life extension factor of 7.3. Note that in this specimen, the pre-crack length was five times greater and σ_{max} was 1.66 times greater compared to the specimens with BCRs and CSCRs.

Fatigue crack growth rate. Since the beginning of the test, the specimens with CF UD and steel crack retarders maintained the crack growth rate below the growth rate of the bare specimen (Fig. 9). Unfortunately, specimens with cold-sprayed crack retarders possessed a higher rate in the entire crack length range, resulting in shorter fatigue life. Although the crack retardation in the 2-Ti64-CSCR specimen can be identified in the (11–28) mm crack length range, the specimen failed earlier than the bare one because the crack grew significantly faster in other regions.

The fatigue crack growth rate in the specimen with one steel layer (1-AISI301-UCCR) was higher in the whole crack length range (Fig. 10(a)), which resulted in shorter fatigue life. On the contrary,

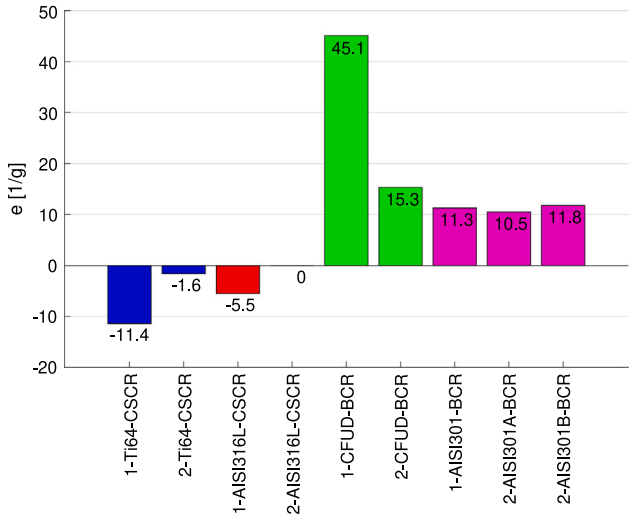

Fig. 11. e factor: bonded and cold-sprayed crack retarders.

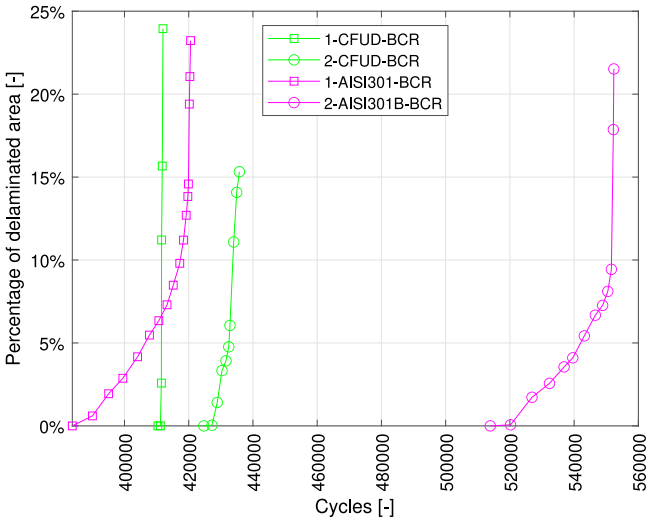

Fig. 12. Delamination growth: bonded crack retarders.

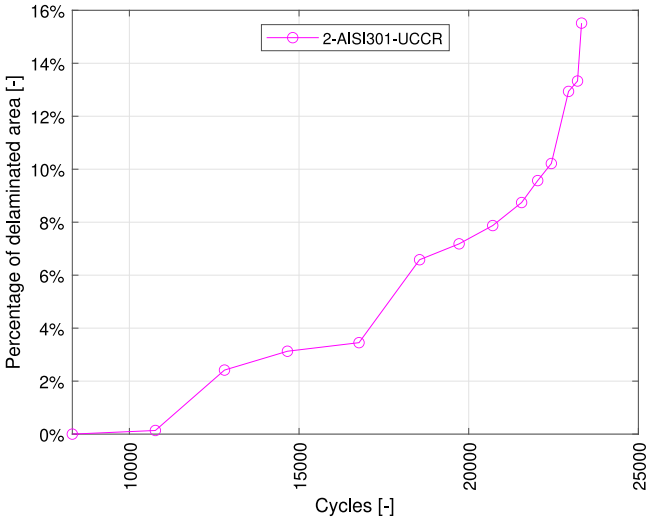

Fig. 13. Delamination growth: ultrasonically consolidated crack retarder.

the specimen with two steel layers possessed fatigue crack growth rate significantly lower compared to the specimen without crack retarders (Fig. 10(b)).

The percentage of life improvement with respect to the bare specimen per unit weight of crack retarder can be expressed by a following parameter:

$$e = \frac{\frac{N_i - N_{bare}}{N_{bare}} 100}{m_{strap}} \tag{2}$$

where m_{strap} is the crack retarder weight. Obviously, the BCR made of two CF UD layers can significantly extend fatigue life while maintaining the relatively low weight of specimen (Fig. 11). One can also observe that the thinner BCRs were much more effective than the thicker ones. This behavior was already proved by Boscolo [19] and Molinari [36]. Specimens with steel BCRs did not perform in the same way. Compared to carbon fiber crack retarders, their total thickness was lower. They probably did not experience secondary bending to the extent that would have lowered performance. The greatest fatigue life increase with respect to the crack retarder unit weight, 82.2% g^{-1}, was observed in the ultrasonically consolidated crack retarder with two steel layers (2-AISI301-UCCR).

Delamination propagation. Each specimen contains two crack retarders and potentially two delaminated areas. Thus, delaminated areas were averaged to obtain delamination growth curves. All bonded crack retarders started delaminating at the end of the specimen's fatigue life. The delamination in specimens with carbon fiber BCRs started later than in specimens with steel BCRs (Fig. 12). The steel crack retarders delaminated with a continually increasing delamination rate. The earlier onset of delamination in specimens with steel crack retarders can be attributed to weaker joint strength. The fracture surface between the CF UD crack retarder and the substrate showed adhesive-cohesive failure. On the contrary, the fracture surface between the steel crack retarder and the substrate was a purely adhesive failure. It suggests that if adhesive bond strength (AISI 301/substrate) is increased, the fatigue retardation effect may be increased.

Although several interface defects were observed in all specimens with CSCRs, the crack retarders did not delaminate. The crack grew directly to the crack retarder without premature delamination, probably due to the poor fatigue properties of the as-sprayed crack retarders. The poor fatigue properties of the cold-sprayed deposits were recently observed by Čížek et al. [37]. In their study, the pure metallic specimens (Ti, Ni, Al and Cu) possessed greater fatigue crack growth rates than their cold-rolled counterparts.

Samely, the ultrasonically consolidated crack retarder (1-AISI301-UCCR) did not delaminate, the crack grew directly into him. Utilizing the ultrasonic consolidation, the joint stiffness was increased and more stress was transferred from the substrate to the crack retarder. Such stress levels allowed the crack to nucleate. The delamination in ultrasonically consolidated crack retarders (Fig. 13) followed a similar trend as in the bonded crack retarders (Fig. 12). Additionally, the delamination in the consolidated crack retarder possessed a triangular shape that is common in the bonded crack retarders[3] [38].

5. Conclusions

This study investigated the crack retarding behavior and delamination progress of bonded, cold-sprayed and ultrasonically consolidated crack retarders. The cold-sprayed (Ti–6Al–4V, AISI 316L) and bonded crack retarders (AISI 301, CF UD) were tested at σ_{max} = 60 MPa, R = 0.1 and f = 15 Hz. The conclusions can be drawn:

[3] Delamination growth in the left crack retarder; 2-AISI301-UCCR specimen and 2-AISI301B-BCR specimen.

1. Stainless steel bonded crack retarders performed better than carbon fiber ones in terms of life extension factor. The most significant increase in fatigue life was identified in specimens with two AISI 301 layers. The greatest percentual life increment with respect to the weight of crack retarder was identified in the specimen with two CF UD layers. However, residual thermal stresses were most likely induced in specimens with carbon fiber crack retarders because a hot curing process was used.
2. Cold-sprayed crack retarders made of 316L and Ti–6Al–4V could not slow down crack propagation. Cold-sprayed deposit formed an integral part with the substrate unlike the adhesively bonded crack retarder. Therefore, the fatigue crack grew directly from the substrate to the cold-sprayed crack retarder. After manufacturing, the most significant out-of-plane deformation was identified in specimens with cold-sprayed crack retarders. Fatigue crack acceleration might be owing to the residual thermal stresses. Because cold-sprayed crack retarders decreased fatigue life and increased the crack growth rate in the substrate, the cold spray technology is not suitable for depositing crack retarders.

Conclusions regarding ultrasonically consolidated crack retarders consisted of one steel layer (AISI 301) tested at σ_{max} = 60 MPa, R = 0.1, f = 15 Hz and two steel layers tested at σ_{max} = 100 MPa, R = 0.1 and f = 15 Hz are subsequently enumerated:

1. Ultrasonically consolidated crack retarder with two steel layers demonstrated the greatest crack retarding effect. A life extension factor of 7.3 was achieved; this corresponded to the life increase with respect to the weight of crack retarder of 82.2% g^{-1}. However, the crack retarder with a single steel layer performed worse than the specimen without crack retarder.
2. Pulsed thermography with thermographic signal reconstruction proved to be the relevant approach to measure delamination extent in ultrasonically consolidated crack retarders. The delamination growth in ultrasonically consolidated crack retarders followed the same trend as in bonded ones. Additionally, triangular delamination was recognized between the substrate and ultrasonically consolidated crack retarder.

Previous studies on crack retarders excluded steels due to the higher specific weight that might result in high fuel consumption and CO_2 emissions of an aircraft. This study filled a knowledge gap on the performance of stainless steel crack retarders manufactured using three distinctive technologies. However, the empirical results reported herein are subject to several limitations. Residual stresses were not measured in any specimen. Bonded and ultrasonically consolidated crack retarders were not examined for potential manufacturing defects. The residual stresses and defects might have a substantial effect on the results. Moreover, galvanic corrosion might be an issue when combining aluminum alloy and carbon fiber crack retarder.

Declaration of competing interest

The authors declare that they have no known competing financial interests or personal relationships that could have appeared to influence the work reported in this paper.

Data availability

The processed thermographic data required to reproduce these findings are available to download from Mendeley Data: http://dx.doi.org/10.17632/xvmwtj8hr9.1.

Acknowledgments

This work was supported by the Internal Grant Agency of Brno University of Technology, Czech Republic (FSI-S-20-6288). The authors thank the Impact Innovations GmbH and Fabrisonic LLC for their constructive suggestions during the planning of this research, Dr. Petr Augustin for assisting with the fatigue crack growth tests and Dr. Petr Kracík for assisting with the thermographic inspection.

Appendix

See Table A.1.

Table A.1
Test matrix.

Specimen name	Crack retarder constituents						Crack retarder			Substrate		Loading parameters	
	No. of layers	Layer	Thickness (t_{lay} [mm])	No. of interlayers	Interlayer	Length [mm]	Width (w_{cr} [mm])	Thickness (t_{cr} [mm])	Manufacturing temperature [°C]	Material and geometry	Dimensions [mm]	Maximum stress (σ_{max} [MPa])	Cyclic loading
Bare	0	–	0	0	–	0	0	0	RT	2024-T351 M(T)	375 × 100 × 2	60	R = 0.1, f = 15 Hz, RT
1-AISI301-BCR	1	AISI 301	0.26	1	Araldite® 2011	200	10	0.44	80			60	
2-AISI301A-BCR	2	AISI 301	0.26	2	Araldite® 2011	200	10	0.60	80			60	
2-AISI301B-BCR	2	AISI 301	0.26	2	Araldite® 2011	200	10	0.55	80			60	
1-CFUD-BCR	2	M10R/38%/UD150/CHS	0.16	1	Araldite® 2011	200	10.2	0.53	80			60	
2-CFUD-BCR	5	M10R/38%/UD150/CHS	0.16	1	Araldite® 2011	200	10.2	1.08	80			60	
1-AISI316L-CSCR	3	AISI 316L	0.20	0	–	200	11.1	0.48	–			60	
2-AISI316L-CSCR	6	AISI 316L	0.20	0	–	200	11.2	0.96	–			60	
1-Ti64-CSCR	3	Ti–6Al–4V	0.20	0	–	200	11.2	0.51	–			60	
2-Ti64-CSCR	6	Ti–6Al–4V	0.20	0	–	200	11.3	1.02	–			60	
Bare	0	–	0	0	–	0	0	0	RT			60	
1-AISI301-UCCR	1	AISI 301	0.26	1	1100-O	200	10.2	0.29	52			60	
Bare	0	–	0	0	–	0	0	0	RT			100	
2-AISI301-UCCR	2	AISI 301	0.26	2	1100-O	200	10.2	0.71	52			100	

References

[1] Nestrenko GI. Comparison of damage tolerance of integrally stiffened and riveted structures. In: 22nd International congress of aeronautical sciences. 2000.

[2] Ritchie R. Mechanisms of fatigue crack propagation in metals, ceramics and composites: role of crack tip shielding. Mater Sci Eng A 1988;103(1):15–28. http://dx.doi.org/10.1016/0025-5416(88)90547-2.

[3] Zhang X, Li Y. Damage tolerance and fail safety of welded aircraft wing panels. AIAA J 2005;43(7):1613–23. http://dx.doi.org/10.2514/1.10275.

[4] Schijve J, Campoli G, Monaco A. Fatigue of structures and secondary bending in structural elements. Int J Fatigue 2009;31(7):1111–23. http://dx.doi.org/10.1016/j.ijfatigue.2009.01.009.

[5] Liljedahl C, Fitzpatrick M, Edwards L. Distortion and residual stresses in structures reinforced with titanium straps for improved damage tolerance. Mater Sci Eng A 2008;486(1–2):104–11. http://dx.doi.org/10.1016/j.msea.2007.09.066.

[6] Schijve J. Crack stoppers and ARALL laminates. Eng Fract Mech 1990;37(2):405–21. http://dx.doi.org/10.1016/0013-7944(90)90050-Q.

[7] Farley G, Newman J, James M. Selective reinforcement to improve fracture toughness and fatigue crack growth resistance in metallic structures. In: 45th AIAA/ASME/ASCE/AHS/ASC structures, structural dynamics & materials conference. 2004, p. 1924. http://dx.doi.org/10.2514/6.2004-1924.

[8] Brot A, Kressel I, Häusler S, Baiz P, Tavares S, Horst P, et al. Analytical and experimental investigations of extending the crack growth life of integrally stiffened aluminum panels by the use of composite material strips. Struct Durab Health Monit 2011;7(3):153–62. http://dx.doi.org/10.3970/sdhm.2011.007.153.

[9] Zhang X, Boscolo M, Figueroa-Gordon D, Allegri G, Irving PE. Fail-safe design of integral metallic aircraft structures reinforced by bonded crack retarders. Eng Fract Mech 2009;76(1):114–33. http://dx.doi.org/10.1016/j.engfracmech.2008.02.003.

[10] Irving PE, Zhang X, Doucet J, Figueroa-Gordon D, Boscolo M, Heinimann M, et al. Life extension techniques for aircraft structures–extending durability and promoting damage tolerance through bonded crack retarders. In: ICAF 2011 structural integrity: Influence of efficiency and green imperatives. Springer; 2011, p. 753–70. http://dx.doi.org/10.1007/978-94-007-1664-3_59.

[11] Ma YE, Liu BQ, Zhao ZQ. The effects of bonded retarder on fatigue crack growth in 7085 Aluminium alloy. In: Advanced materials research. 2011;vol. 217:1135–40. http://dx.doi.org/10.4028/www.scientific.net/AMR.217-218.1135.

[12] Jones R, Matthews N, Rodopoulos C, Cairns K, Pitt S. On the use of supersonic particle deposition to restore the structural integrity of damaged aircraft structures. Int J Fatigue 2011;33(9):1257–67. http://dx.doi.org/10.1016/j.ijfatigue.2011.03.013.

[13] Hehr A, Wenning J, Norfolk M, Sheridan J, Newman JA, Domack M. Selective reinforcement of aerospace structures using ultrasonic additive manufacturing. J. Mater. Eng. Perform. 2018;1–8. http://dx.doi.org/10.1007/s11665-018-3614-1.

[14] Colavita M, Bowler A, Zhang X, Irving PE. Adhesively bonded CFRP straps as fatigue crack growth retarders on AA2024-T3. In: Proceedings of SAMPE conference 2006. 2006.

[15] Liljedahl C, Fitzpatrick M, Edwards L. Evolution of residual stresses with fatigue crack growth in integral structures with crack retarders. Mater Sci Eng A 2009;523(1–2):152–9. http://dx.doi.org/10.1016/j.msea.2009.06.024.

[16] Liljedahl C, Fitzpatrick M, Zanellato O, Edwards L. Effect of temperature on the residual stresses in an integral structure with a crack-retarding patch. Strain 2011;47:293–8. http://dx.doi.org/10.1111/j.1475-1305.2010.00768.x.

[17] Syed AK, Fitzpatrick ME, Moffatt JE, Doucet J, Durazo-Cardenas I. Effect of impact damage on fatigue performance of structures reinforced with GLARE bonded crack retarders. Int J Fatigue 2015;80:231–7. http://dx.doi.org/10.1016/j.ijfatigue.2015.06.006.

[18] Syed AK. Durability of bonded crack retarders for aerospace [Ph.D. thesis], The Open University; 2014.

[19] Boscolo M, Allegri G, Zhang X. Design and modelling of selective reinforcements for integral aircraft structures. AIAA J 2008;46(9):2323–31. http://dx.doi.org/10.2514/1.35712.

[20] Papyrin A, Kosarev V, Klinkov S, Alkhimov A, Formin VM. Cold spray technology. Amsterdam, Netherlands: Elsevier; 2007.

[21] White D. Ultrasonic object consolidation. 2003, Patent no. 6519500.

[22] Wolcott PJ, Sridharan N, Babu SS, Miriyev A, Frage N, Dapino MJ. Characterisation of Al–Ti dissimilar material joints fabricated using ultrasonic additive manufacturing. Sci Technol Weld Join 2016;21(2):114–23. http://dx.doi.org/10.1179/1362171815Y.0000000072.

[23] Obielodan J, Stucker B, Martinez E, Martinez J, Hernandez D, Ramirez D, et al. Optimization of the shear strengths of ultrasonically consolidated Ti/Al 3003 dual-material structures. J Mater Process Technol 2011;211(6):988–95. http://dx.doi.org/10.1016/j.jmatprotec.2010.12.017.

[24] Sova A, Grigoriev S, Okunkova A, Smurov I. Cold spray deposition of 316L stainless steel coatings on aluminium surface with following laser post-treatment. Surf Coat Technol 2013;235:283–9. http://dx.doi.org/10.1016/j.surfcoat.2013.07.052.

[25] ASM Handbook, Volume 2: Properties and selection: Nonferrous alloys and special-purpose materials. Materials Park, Ohio: ASM International; 1990, http://dx.doi.org/10.31399/asm.hb.v02.9781627081627.

[26] Dymáček P, Klement J. Properties and manufacturing of steel-C/epoxy fiber-metal laminates. In: Proceedings of the fourth seminar on recent research and design progress in aeronautical engineering and its influence on education: Part II. Institute of Aeronautics and Applied Mechanics; 2011, p. 47–52.

[27] ASM handbook, volume 1: Properties and selection: Irons, steels, and high-performance alloys. Materials Park, Ohio: ASM International; 1990, http://dx.doi.org/10.31399/asm.hb.v01.9781627081610.

[28] Hexcel. HexPly® M10R. 2015.

[29] Huntsman Advanced Materials. Araldite® 2011 (AW106 + HW953U): Two component epoxy paste adhesive. 2004.

[30] ASTM E647-15 standard test method for measurement of fatigue crack growth rates. 2022.

[31] Sandvik Materials. Austenitic stainless steel metal powder. 2019, https://www.materials.sandvik/cz/produkty/metal-powder/list-of-materials/austenitic-stainless-steels/.

[32] AP&C. Ti-6al-4V (15-45 μm). 2019, http://advancedpowders.com/nos-poudres-atomisees-au-plasma/produits/ti-6al-4v-poudre-dalliage-de-titane/#15-45_m.

[33] ASM specialty handbook: Aluminum and aluminum alloys. Materials Park, Ohio: ASM International; 1993.

[34] Hehr A, Norfolk M. A comprehensive review of ultrasonic additive manufacturing. Rapid Prototyp J 2019. http://dx.doi.org/10.1108/RPJ-03-2019-0056.

[35] Obielodan J, Ceylan A, Murr L, Stucker B. Multi-material bonding in ultrasonic consolidation. Rapid Prototyp J 2010. http://dx.doi.org/10.1108/13552541011034843.

[36] Molinari G, Meneghin I, Melega M, Troiani E. Parametric damage tolerance design of metallic aeronautical stiffened panels. Aeronaut J 2012;116(1182):815–31. http://dx.doi.org/10.1017/S0001924000007296.

[37] Cizek J, Kovarik O, Cupera J, Kondas J, Bajer T, Siska F, et al. Measurement of mechanical and fatigue properties using unified, simple-geometry specimens: Cold spray additively manufactured pure metals. Surf Coat Technol 2021;412:126929. http://dx.doi.org/10.1016/j.surfcoat.2021.126929.

[38] Vaclav Jetela. Data for: Bonded and additively manufactured crack retarders: A comparative study of damage tolerance properties. Mendeley Data; 2022, http://dx.doi.org/10.17632/xvmwtj8hr9.1, V1.